Michael E. Mann | Stefan Rahmstorf | Kai Kornhuber |
Byron A. Steinman | Sonya K. Miller | Stefan Petri | Dim Coumou

Projected changes in persistent extreme summer weather events

The role of quasi-resonant amplification

Suggested citation referring to the original publication:
Science Advances 4 (2018) 10, Art. eaat3272
DOI https://doi.org/10.1126/sciadv.aat3272
ISSN (online) 2375-2548

CLIMATOLOGY

Projected changes in persistent extreme summer weather events: The role of quasi-resonant amplification

Michael E. Mann[1]*, Stefan Rahmstorf[2,3], Kai Kornhuber[2], Byron A. Steinman[4], Sonya K. Miller[1], Stefan Petri[2], Dim Coumou[2,5]

Persistent episodes of extreme weather in the Northern Hemisphere summer have been associated with high-amplitude quasi-stationary atmospheric Rossby waves, with zonal wave numbers 6 to 8 resulting from the phenomenon of quasi-resonant amplification (QRA). A fingerprint for the occurrence of QRA can be defined in terms of the zonally averaged surface temperature field. Examining state-of-the-art [Coupled Model Intercomparison Project Phase 5 (CMIP5)] climate model projections, we find that QRA events are likely to increase by ~50% this century under business-as-usual carbon emissions, but there is considerable variation among climate models. Some predict a near tripling of QRA events by the end of the century, while others predict a potential decrease. Models with amplified Arctic warming yield the most pronounced increase in QRA events. The projections are strongly dependent on assumptions regarding the nature of changes in radiative forcing associated with anthropogenic aerosols over the next century. One implication of our findings is that a reduction in midlatitude aerosol loading could actually lead to Arctic de-amplification this century, ameliorating potential increases in persistent extreme weather events.

INTRODUCTION

A series of persistent, extreme, and costly summer weather events over the past decade and a half, including the 2003 European heat wave, 2010 Pakistan flood/Russian heat wave, 2011 Texas drought, 2013 European floods, 2015 California wildfires, and 2016 Alberta wildfires have led to ongoing discussion in the scientific literature regarding the relationship between anthropogenic climate change and warm-season weather extremes (*1*–*27*). Some increases in summer weather extremes can be explained by relatively straightforward thermodynamic processes, e.g., upward shifts in the temperature distribution leading to increases in the frequency of heat waves (*1*, *2*, *5*, *12*, *13*) or the influence of a warming atmosphere on intense precipitation events (*10*, *15*, *16*). A growing number of studies (*3*, *7*, *8*, *11*, *14*–*16*, *18*–*20*, *22*, *23*, *26*–*28*), however, suggest that mechanisms involving atmospheric dynamics are necessary to explain the characteristics—particularly the unusually persistent and amplified disturbances in the jet stream—that are associated with persistent extreme summer weather events.

A specific mechanism involving the characteristics of atmospheric Rossby (or "planetary") waves may be implicated in some of these cases (*11*, *14*, *22*, *26*–*28*). Charney and De Vore (*29*) used a simple barotropic channel model to demonstrate the potential for resonance of stationary planetary waves, while Hoskins and Karoly (*30*) and Hoskins and Ambrizzi (*31*) demonstrated the potential for waveguide-like behavior for stationary planetary waves. Petoukhov *et al.* (*11*, *22*) demonstrated that planetary waves within the synoptic wave number range (wave numbers 6 to 8) can become effectively trapped in a latitudinal waveguide depending on the meridional profile of the midlatitude westerly jet, thus providing a mechanism for the time dependence of resonant behavior, because that profile exhibits substantial variability in time. If these waveguide conditions hold, then a pronounced amplification of waves that are excited by orographic or thermal forcing can occur (*32*). This phenomenon is referred to as quasi-resonant amplification (QRA).

While the detailed mechanisms are explored in depth elsewhere (*11*), we provide a brief summary. Starting with the linearized quasi-geostrophic barotropic potential vorticity equation, we have, in the weak perturbation ("WKB") limit, the approximate description of the mid-troposphere (300 to 500 mbar) streamfunction ψ as a function of latitude ϕ and longitude λ

$$\left(\frac{\partial}{\partial t}+\frac{\bar{u}}{a\cos\varphi}\frac{\partial}{\partial\lambda}\right)\Delta\psi+\left(2\Omega-\frac{\Delta\bar{u}}{a\cos\varphi}\right)\frac{\partial\psi}{\partial\lambda}=V_T+V_O-V_F \quad (1)$$

where V_T is the thermal forcing, V_O is the orographic forcing, V_F represents frictional damping, $\bar{u}$ is the mean zonal velocity, a is Earth's radius, Ω is Earth's rotational angular velocity, and t is time.

The equation yields plane wave free solutions (i.e., with right-hand side of Eq. 1 set to zero)

$$\psi = e^{i(kx+ly-\omega t)} \quad (2)$$

where k is the zonal wave number, l is the meridional wave number, ω is the frequency of zonally propagating waves, and t is time.

For persistent atmospheric states, we are interested in stationary (ω = 0) solutions. The dispersion relation ω = ω(l,k,ϕ) then yields (assuming $u > 0$)

$$l^2=\frac{2\Omega\cos^3\varphi}{a\bar{u}}-\frac{\cos^2\varphi}{a^2\bar{u}}\frac{d^2\bar{u}}{d\varphi^2}-\frac{\sin\varphi\cos\varphi}{a^2\bar{u}}\frac{d\bar{u}}{d\varphi}+\frac{1}{a^2}-\frac{k^2}{a^2} \quad (3)$$

The key observation is that l^2 can exhibit two turning points, i.e., zero crossings near latitudes of roughly 30°N and 45°N. These

[1]Department of Meteorology and Atmospheric Science, Pennsylvania State University, University Park, PA, USA. [2]Earth System Analysis, Potsdam Institute for Climate Impact Research, Potsdam, Germany. [3]Institute of Physics and Astronomy, University of Potsdam, Potsdam, Germany. [4]Department of Earth and Environmental Sciences and Large Lakes Observatory, University of Minnesota Duluth, Duluth, MN, USA. [5]Institute for Environmental Studies (IVM), VU University Amsterdam, Amsterdam, Netherlands.
*Corresponding author. Email: mann@psu.edu

conditions occur for certain meridional profiles of $\bar{u}$—particularly for a double-peaked westerly jet characterized by strengthened westerlies in subtropical and subpolar latitudes and weakened westerlies in midlatitudes—and over the restricted wave number range $k = 6$ to 8. Outside the turning points, l^2 becomes negative and meridionally propagating solutions are not permitted, preventing dispersion of wave energy to higher or lower latitudes and yielding a zonally directed waveguide for $k = 6$ to 8. A persistent subtropical turning point can be created when the zonal mean westerlies are in a double jet state (*26*, *28*). This state is characterized by a high-latitude Arctic front jet and a confined and steep subtropical jet, which is instrumental in creating a subtropical turning point. It is well documented that these jet configurations are efficient waveguides (*33*).

If the waveguide is (almost) circumglobal, then wave energy is efficiently trapped and waves constructively interfere with the forcing, leading to resonance. Trapped planetary waves with $k = 6$ to 8 that are excited by thermal or orographic forcing will tend to grow in amplitude. The waveguide condition depends only on the zonal wave number k and the shape of the zonal mean zonal wind ($\bar{u}$) profile. Through the thermal wind relationship, this profile can, in turn, be tied to meridional temperature gradients in the lower troposphere. Although a zonal mean approach neglects regional variations in the zonal flow, it has shown to be suitable for assessing the "waveguidability" of jets (*11*, *33*).

As the derivation of the fundamental equations requires a certain degree of idealization, there are some caveats with this conceptual development. As QRA-related disturbances grow sufficiently in amplitude, they become baroclinically unstable and the barotropic assumption (and WKB approximation) is violated. Our zonal mean approach neglects longitudinal variations in the zonal flow and the possibility of meridionally oriented waveguides. Nonetheless, the theoretical framework presented above is useful for understanding the conditions under which QRA is likely to arise. The reader is referred to the studies of Petoukhov *et al.* (*11*, *22*) for empirical support for the approximate validity of this conceptual model for QRA, as well as limitations and caveats of the mechanism.

Petoukhov *et al.* (*11*) demonstrated that QRA likely played a key role in several damaging, extreme, and persistent weather events including the 2003 European heat wave, 2010 Russian heat wave/fires and Pakistan flood, and 2011 Oklahoma/Texas heat wave and drought. Other subsequent studies (*14*, *18*, *22*, *26*, *28*) have demonstrated the likely role of QRA in a host of other recent extreme warm-season weather events. Kornhuber *et al.* (*26*) showed that QRA explains roughly a third of all high-amplitude events with wave numbers 6 to 8 and that amplitudes of quasi-stationary waves of that wave number range are significantly higher when resonance conditions are met. They also showed that planetary waves amplified by QRA exhibit specific preferred phases due to the characteristic stationary orographic forcing of the Northern Hemisphere midlatitudinal orographic profile. Their analysis shows that central United States and western Europe are specifically susceptible for persistent heat waves during QRA episodes (*28*).

Coumou *et al.* (*14*) argued that an increase in QRA events during the satellite reanalysis era (1979–2011) coincides with a measure of Arctic amplification (AA) of warming. This amplification is expected from various feedbacks including the ice-albedo feedback associated with anthropogenic greenhouse warming. While both the polar and subtropical boundaries of the waveguide are important, it is the former that is strongly affected by this amplified warming. Because upper-level westerlies are tied to a negative meridional gradient (i.e., colder toward the pole) in lower tropospheric temperatures through the thermal wind relationship, AA of warming would seem to imply reduced upper-level midlatitude westerlies ($\bar{u}$), potentially favoring occurrence of QRA.

We see through Eq. 3 that the actual wave dynamics underlying QRA are dependent on the second derivative of the mean zonal wind with latitude ($d^2u/d\phi^2$). Even modest model biases in u are likely to propagate into considerably larger biases upon two successive differentiations, making it challenging for even state-of-the-art climate models to correctly model this quantity. Thus, the actual wave dynamics behind QRA are unlikely to be faithfully resolved by the models. Mann *et al.* (*27*) (henceforth "M17") therefore instead developed an indirect observationally based fingerprint for QRA conditions based on meridional surface temperature profiles. As shown by Petoukhov *et al.* (*11*), there is a robust relationship between surface/lower atmosphere temperature gradients and upper-level zonal winds in the regions critical to QRA, and there is a clear signature for the various key QRA events noted of the past few decades. These profiles are governed substantially by large-scale radiative forcing and are likely to yield a robust metric when applied to climate model simulations, yet are closely tied to QRA through the thermal wind mechanism as discussed above.

To test whether this indirect approach to assessing QRA in models is more reliable than a direct analysis of QRA events in the model simulations, we have performed an analysis across the Coupled Model Intercomparison Project Phase 5 (CMIP5) multimodel historical ensemble used in this study (see Materials and methods) to examine the relative faithfulness with which the two respective quantities, i.e., $T(\phi)$ and $d^2u(\phi)/d\phi^2$, are reproduced in the climate models relative to (reanalysis) observations. We observe a small ensemble mean error of roughly 0.5% for $T(\phi)$ [or, alternatively, a still modest roughly 27% ensemble mean error for $dT(\phi)/d\phi$]. For comparison, we obtain a quite large 344% error for $d^2u(\phi)/d\phi^2$ (see fig. S1). We conclude that our indirect approach, wherein the $T(\phi)$ profile is used as a proxy for QRA behavior in the models, can yield meaningful results, while direct assessment of QRA behavior is not possible using currently available multimodel ensemble simulations. One assumption of our approach, of course, is that the fingerprint as established in historical observations remains valid in the future. Related to that assumption is the assumption that the structure of planetary waves excited by orographic or thermal forcing remains similar in the future.

Using European Centre for Medium-Range Weather Forecasts (ECMWF) reanalysis data (ERA) confined to the midlatitude (25°N to 75°N) region of interest (*28*) and the QRA detection scheme described above and developed previously (*26*), M17 produced a composite of boreal summer [June to August (JJA)] zonally averaged near-surface (1000 hPa) temperature profiles associated with QRA-favorable time intervals. Differencing the QRA-favorable and climatological mean profiles, they defined an anomalous meridional temperature "fingerprint" associated with QRA conditions, onto which polar-amplified warming projects positively (although there is additional structure in the fingerprint related to, e.g., land/ocean contrast). Examining the trend over time in this fingerprint in both long-term historical observations and the CMIP5 historical model simulations (table S1), they found consistent evidence for an increase in QRA-favorable conditions.

RESULTS

Here, we extend the M17 analysis by examining the behavior of the QRA fingerprint in future climate projections (Fig. 1). The fingerprint (Fig. 1A) exhibits negative values in the subtropics, increases to near-neutral values at 40°N, a decline toward more negative values through

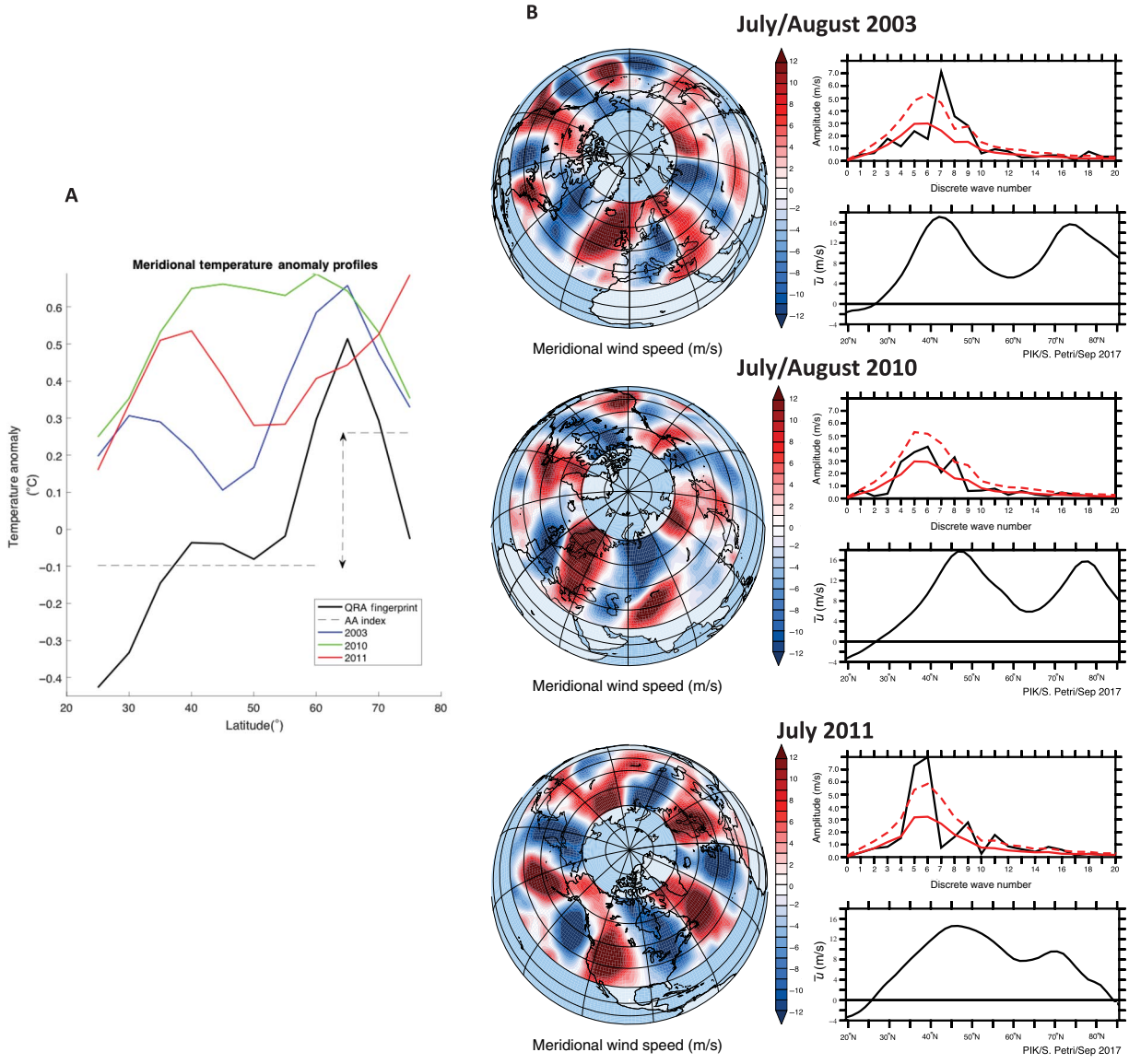

Fig. 1. QRA fingerprint and QRA event signatures. (**A**) JJA 1000-hPa meridional temperature anomalies over the extratropical region 25°N to 75°N associated with QRA-favorable conditions (i.e., QRA fingerprint) based on composite of events from ERA reanalysis data (1979–2015) along with the actual JJA meridional surface temperature anomalies corresponding to three selected QRA events (July/August 2003, July/August 2010, and August 2010). (**B**) Upper-troposphere (300 hPa) meridional wind, zonal wave number spectra (computed for the meridional average over 37.5°N to 57.5°N; the climatological mean spectra and associated 1.5σ upper limit are shown for comparison by red solid and red dashed curves, respectively), and zonal mean zonal wind profiles associated with each of the three aforementioned events.

50°N, and pronounced positive values again at higher subpolar latitudes. The JJA meridional temperature profiles associated with several prominent recent QRA-influenced extreme weather events (2003 European heat wave, 2010 Russian wildfires/Pakistan floods, and 2011 Oklahoma/Texas heat wave and drought) are also shown (Fig. 1A) along with the large-scale 300-hPa meridional wind fields, zonal wave number spectra, and zonal mean zonal wind profiles associated with the three events, each of which exhibits the expected QRA features (Fig. 1B; note, for example, the spectral peaks in the $k = 6/7/8$ range and the double-peaked latitudinal structure in the zonal winds).

We see how each of the three events is associated with a prominent wave 6/7/8 pattern, and a summer mean meridional temperature profile that projects substantially onto the QRA fingerprint. The correlations with the fingerprint are $r = 0.79$, $r = 0.63$, and $r = 0.41$, respectively, which are statistically significant at the $P < 0.001$, $P < 0.02$, and $P < 0.1$ levels, respectively. Superimposed on the seasonal mean temperature profiles is considerable intraseasonal variation, and the positive projection of the seasonal mean temperature profiles onto the QRA fingerprint substantially increases the likelihood of daily-to-weekly temperature profiles that closely resemble the QRA fingerprint.

Arctic-amplified warming projects onto this latitudinal anomaly pattern. However, the fingerprint has considerably more latitudinal structure than a simple index (65N to 75N mean minus 25N to 60N mean temperatures) of AA (see Fig. 1A). Thus, while we might expect some broad similarity in the behavior of the QRA fingerprint and AA index, we might also expect some significant differences. The anomalous

meridional temperature gradient associated with the QRA profile is characterized by a large positive peak in the midlatitude zone of 50°N to 65°N, which, via thermal wind, implies a more-pronounced minimum in the zonal mean zonal wind. More poleward (i.e., beyond 65°N), the reduction in the temperature gradient (and thus a stronger negative gradient) implies stronger westerlies in subpolar regions. As noted earlier, these are precisely the double-peaked jet conditions associated with QRA.

The next step in the analysis involves projecting the CMIP5 simulation meridional temperature profiles onto the QRA fingerprint

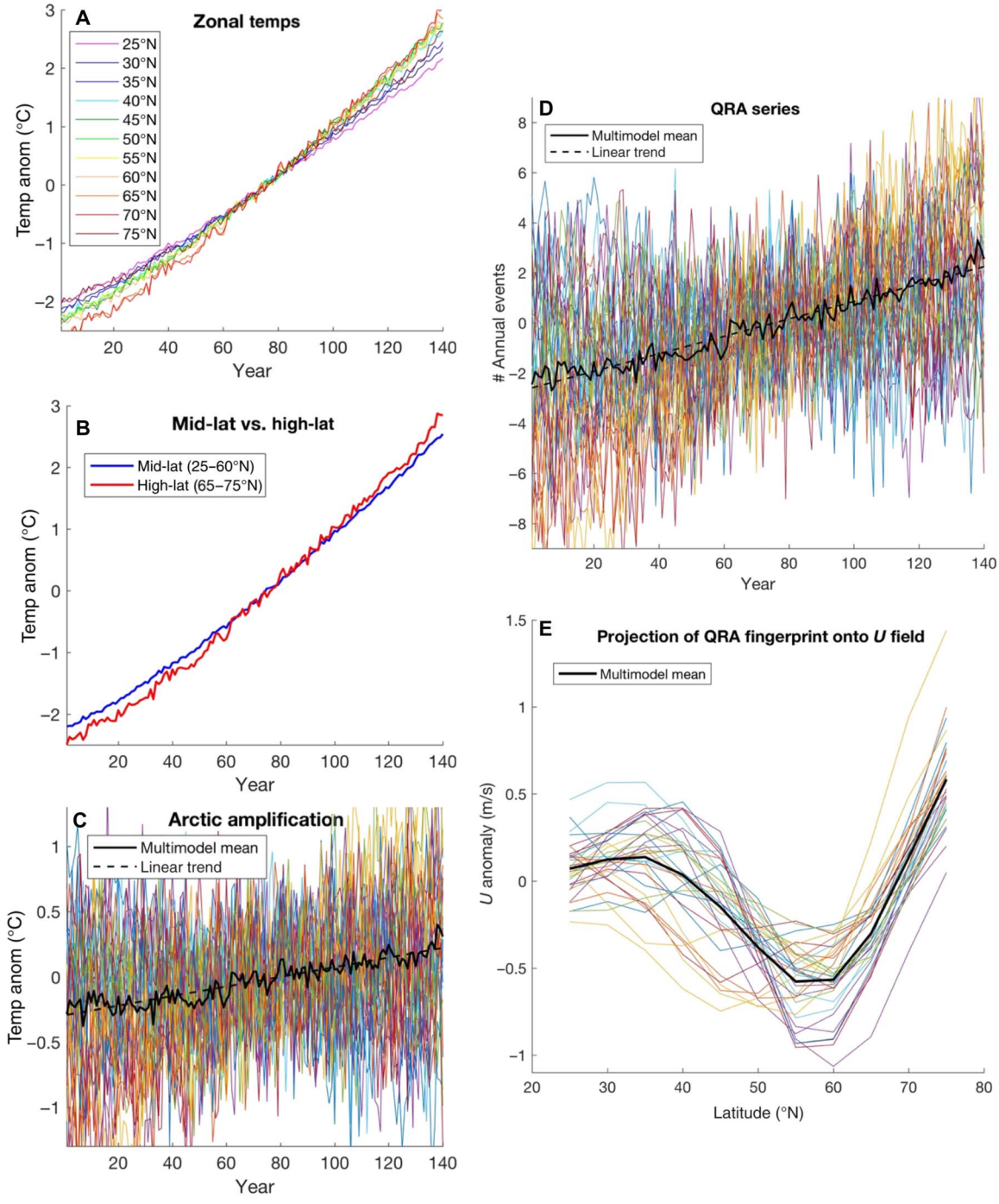

Fig. 2. Analysis of 1PCTCO2 experiments (JJA seasonal means). (**A**) Time series of multimodel average zonal mean temperature anomalies. (**B**) Comparison of multimodel average midlatitude (25°N to 60°N) and high-latitude (65°N to 75°N) mean temperature anomalies. (**C**) AA index defined as high-latitude minus midlatitude series including individual simulations shown (colored curves) and multimodel mean (black solid curve), along with linear trend (black dashed lines). (**D**) QRA series for individual series and multimodel mean [conventions as in (C); see Materials and methods for details on scaling of QRA]. (**E**) Projection of the QRA fingerprint onto zonal wind anomalies.

(see Fig. 1A) using linear regression (see Materials and methods). In assessing the impact of projected future climate change on the conditions favoring QRA, it is instructive to first examine the simple case (Fig. 2) of linearly increasing greenhouse forcing with no other changes in external forcing. We use steady CO_2 increase experiments of the CMIP5 ensemble ($N = 35$ simulations, $M = 26$ models; see table S2 for details), which are initialized by a preindustrial control and subject to a 1%/year increase in CO_2 (henceforth "1PCTCO2").

Examining the multimodel ensemble mean JJA surface temperatures, we see the expected polar amplification of warming with latitude

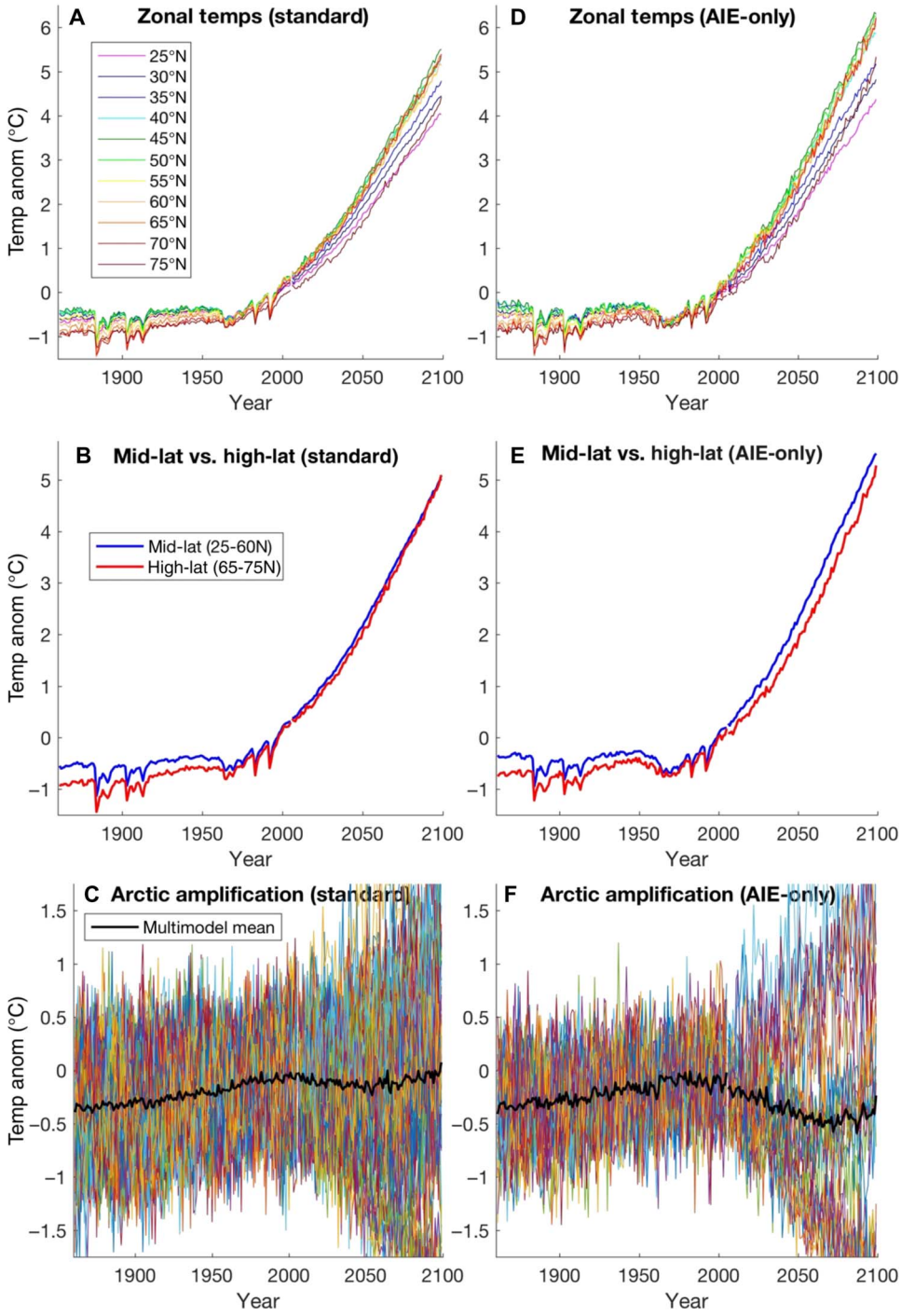

Fig. 3. Analysis of RCP8.5 future projections (JJA seasonal means). Included are both (**A** to **C**) full multimodel ensemble and (**D** to **F**) AIE-only sub-ensemble (JJA seasonal means). (A and D) Time series of multimodel average zonal mean temperature anomalies. (B and E) Comparison of multimodel mean midlatitude (25°N to 60°N) and high-latitude (65°N to 75°N) mean temperature anomalies. (C and F) AA index defined as high-latitude minus midlatitude series (colored curves, individual simulations; black curves, multimodel mean).

(Fig. 2A), with summer (JJA) warming in the high-latitude zone (65°N to 75°N) substantially exceeding that for the midlatitude zone (25°N to 60°N) (Fig. 2B). The multimodel mean AA index (Fig. 2C) shows a nearly linear increase over time. There is spread within the multimodel ensemble [with two-thirds (67%) of the ensemble members displaying AA]. We next examine the QRA fingerprint series [Fig. 2D; the unitless QRA index has been scaled against the actual historical series of annual QRA event numbers (see Materials and methods) for the purpose of defining the vertical scale]. This series displays an even more robust positive trend [in this case, more than three-fourths (76%) of the ensemble members display a positive trend], consistent with the hypothesis (see M17) that climate change attributes other than AA—particularly the enhanced land/ocean contrast and perhaps changing snow cover (*8*), as expressed in the corresponding zonal means—also project positively onto the QRA fingerprint. The projection of the 300-hPa *U* field (Fig. 2E) onto the QRA series shows the expected (M17) anomaly pattern of weakened midlatitude westerlies and strengthened subpolar and subtropical westerlies indicative of the double-peaked jet associated with QRA-favorable conditions. The observed ~2 m/s peak-to-peak amplitude of the response is consistent with a simple calculation based on the thermal wind approximation (see Materials and methods).

We then examined the CMIP5 future (2006–2100) projections (see Materials and methods for details). We focus on the RCP (Representative Concentration Pathway) 8.5 experiments ($N = 73$ simulations, $M = 39$ models; see table S3), which reflect a "business-as-usual" scenario of steadily increasing carbon emissions through the end of the 21st century, but with a sharp drop-off in anthropogenic sulfate aerosol production over the next half century (reflecting the assumption of a transition to "cleaner" coal burning in the developing world). Results for the RCP 2.6 scenario (table S4), which reflects more ambitious carbon emission reductions, yield qualitatively similar results but with substantially smaller future projected changes (see figs. S2 and S3).

We combine the projections and the previously assessed (M17) CMIP5 historical (1880–2005) simulations ($N = 164$, $M = 48$; see table S1) to provide a historical context for the future projections. We analyze both the full multimodel ensembles and the aerosol indirect effects (AIE) subsets of the ensembles consisting only of models that include both aerosol first and second indirect effects ($N = 46$ historical simulations and $N = 28$ future simulations) to better assess the potentially important role played by anthropogenic aerosols.

DISCUSSION

In contrast with the 1PCTCO2 simulations, the RCP 8.5 projections (Fig. 3) show no clear pattern of polar amplification of summer warming. This effect is particularly pronounced in the AIE simulations (Fig. 3, A and B). Only 46% of the multimodel simulations (less than half) and an even lower 32% (less than a third) of the AIE simulations exhibit positive polar amplification. This underappreciated feature of the climate projections is readily understood as a consequence of projected changes in anthropogenic aerosol forcing.

There is a marked decrease in summer season aerosol forcing over the early 21st century as aerosols ramp down sharply, the response to which is especially large during the summer season when solar insolation is high and especially pronounced in midlatitudes where aerosol production takes place. This positive trend in radiative forcing in midlatitudes during the first half of the 21st century is of similar magnitude to the positive greenhouse forcing trend (~1 W/m^2) and yields prominent warming in the midlatitudes relative to subpolar latitudes, i.e., an Arctic de-amplification. Over the latter half of the 21st century, as the aerosol trend is minimal, greenhouse forcing dominates, and the trend returns toward AA. This effect is seen as an inflection in the AA index in the mid-21st century (Fig. 3C). We can also see this effect in the spatial pattern of first-half 21st century surface temperature trends, which displays especially prominent warming over the midlatitude continents in the ensemble mean and especially in the subset of models that are most negative QRA trending (Fig. 4).

We are now in a position to understand the behavior observed in the QRA fingerprint series (Fig. 5). For the full multimodel ensemble mean, we see a slowdown in the increasing trend over the first half of the 21st century, followed by an acceleration in the late 21st century. In the case of the AIE subset, we see a flat (actually, very slightly negative) trend over the first half of the 21st century, followed by a very rapid increase over the latter 21st century. A slim majority (59%) of the multimodel

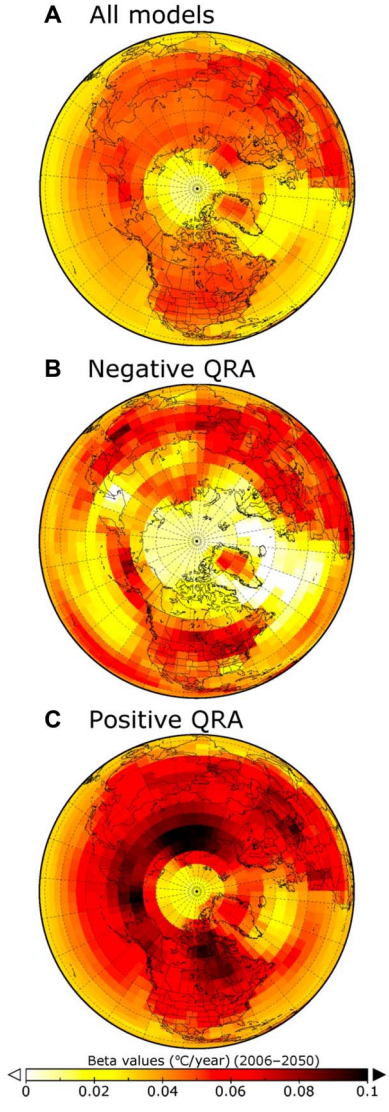

Fig. 4. Mean surface temperature trend patterns (JJA seasonal means) over 2006–2050. (**A**) multimodel ensemble, (**B**) most negative QRA-trending ensemble members, and (**C**) most positive QRA-trending ensemble members ("most" is defined as upper 10th percentile of multimodel ensemble).

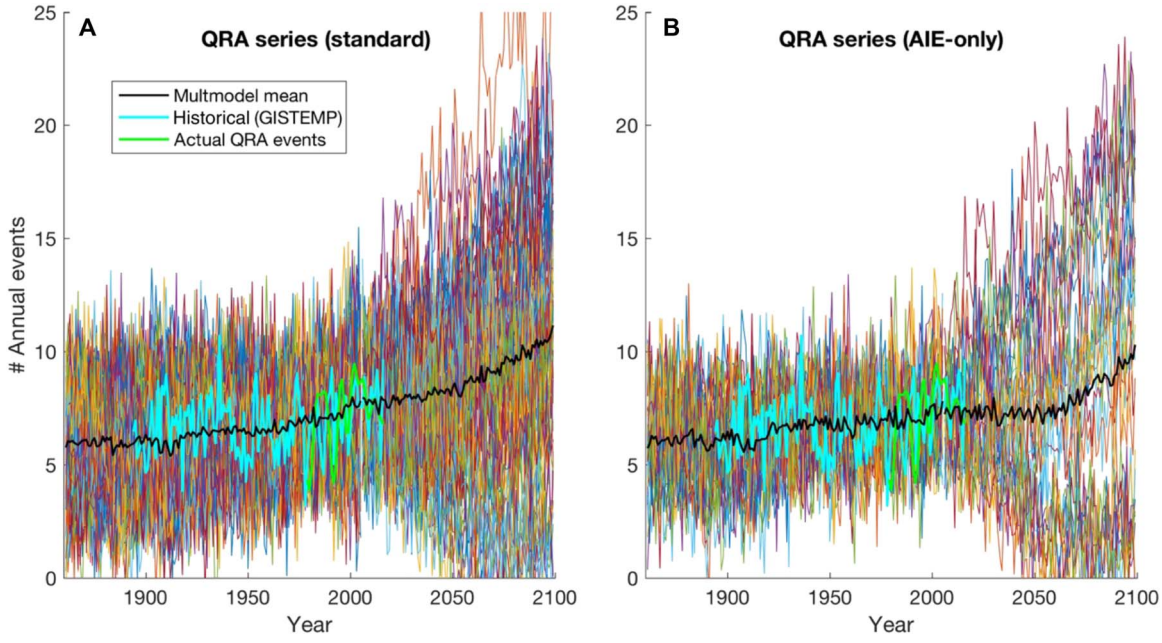

Fig. 5. QRA fingerprint series for RCP8.5 future projections. Both (**A**) full multimodel ensemble and (**B**) AIE-only sub-ensemble. Conventions are as in Fig. 3D. The historical QRA series calculated from [Goddard Institute for Space Studies Surface Temperature Analysis (GISTEMP)] surface temperature observations from 1894 to 1916 (cyan) and the actual series of annual QRA event counts (green) from 1979 to 2015 (as diagnosed from ERA reanalysis data; see Materials and methods for further details) are shown for comparison.

simulations exhibit an increase in the QRA fingerprint during the first half of the 21st century, while there is an equal split (50%) between increasing and decreasing QRA among the AIE simulations.

These trends reflect a competition between the overall influence of greenhouse warming on QRA, which, as we have seen before (Fig. 2), is a steady increase in QRA, and the mitigating effects of decreasing aerosol forcing, which dominates in the first half of the 21st century and is most prominent in the AIE-only simulations. The models that exhibit the greatest decline in the QRA fingerprint series during the first half of the 21st century are the models that display especially pronounced midlatitude warming during that period (Fig. 4) from decreasing aerosols.

In both cases, however, by the end of the 21st century, the impact of greenhouse warming is dominant, and we observe an increase in 64% of the full multimodel ensemble simulations and 74% of the AIE-only simulations (the number is higher in this case because many of the models must recover from a prominent aerosol-induced decrease during the first half of the century). In terms of the actual number of QRA events, we project an average increase from the current historical level of ~7.5 events/year to ~11 events/year, i.e., a roughly 50% increase in the annual number of events, for the full multimodel ensemble. In some individual models, however, the increase is far greater (Fig. 5), i.e., more than a tripling by 2100 (Fig. 5). These models tend (see Fig. 4C) to be those where greenhouse-induced high-latitude amplification dominates. It is apparent that the treatment of anthropogenic aerosols plays a key role in determining the pathway of QRA changes over the next century.

CONCLUSION

Our previous work (M17) demonstrated a greenhouse warming–related increasing trend in occurrence of QRA-favorable conditions associated with devastating recent extreme summer weather events including the 2003 European heat wave, the 2010 Pakistan flood and Russian heat wave, and the 2011 Texas and Oklahoma heat wave and drought. The analysis we have presented here indicates that anthropogenic warming will likely lead to future increases in these events under business-as-usual burning of fossil fuels, keeping in mind our assumption that the historically defined fingerprint remains valid in the future climate. How substantial those increases are, and the historical path they follow—particularly during the first half of the 21st century—depends substantially on the prominence of midlatitude warming arising from decreasing aerosols. Given the divergent nature of the CMIP5 multimodel simulations with regard to this feature, any evaluation of risk should take into account not only the mean expected increase (~50%) in events but also the possibility of a far larger (i.e., roughly tripling) number of events, as suggested by some of the model simulations. An important implication of our findings is that a reduction in aerosol load may provide the additional benefit of preventing or ameliorating changes in midlatitude temperature gradients that favor an increase in persistent extreme summer weather events.

MATERIALS AND METHODS

QRA fingerprint

To define the QRA meridional temperature fingerprint, we used the QRA detection scheme developed by Kornhuber *et al.* (*26*) applied to temperature profiles as in M17 using the JJA 1979–2015 ERA interim reanalysis (2.5° × 2.5°). Near-surface atmospheric temperature profiles were calculated using z = 1000 hPa daily data over the full Northern Hemisphere (0°N to 90°N) in 37 steps (2.5°). We focused on long-duration (≥10 days) wave number 7 events to define QRA-favorable time intervals and confined zonal mean profiles to the latitude range (25°N to 75°N) of interest. The fingerprint was interpolated to a

5° latitude to be consistent with the grid of the model simulations and observational datasets (see below) and centered on zero. This yields an 11-element zero-centered row vector that defines the QRA fingerprint.

The QRA fingerprint is found to be robust with respect to sampling considerations. Calculating the fingerprint based on either the first half (1979–1997) or second half (1998–2015) of the full ERA dataset yields profiles that are very similar to those based on the full (1979–2015) data interval (fig. S4).

The projection of other fields onto the QRA fingerprint was estimated in both CMIP5 simulated (see below) and observational (see below) datasets by calculating the linear inner product of those fields and the QRA fingerprint defined above.

We also calculated the time series of observed annual QRA events using the set of all QRA events, with wave numbers 6 to 8 detected in the ERA reanalysis dataset over 1979–2015 (*14*). Owing to the noisy nature of this count series, it was smoothed using an interannual smoothing filter ($f = 0.2$ cycle/year cutoff) for the purpose of comparison with other calculated QRA series. We used mean and variance matching with this series to scale the observational and model-based QRA fingerprint series in dimensions of equivalent annual number of QRA events.

CMIP5 historical simulations

We used the CMIP5 historical experiment (*34*) multimodel ensemble simulations, including both the anthropogenic + natural forced simulations ($N = 164$ realizations, $M = 48$ models) and anthropogenic-only forced simulations ($N = 40$ realizations, $M = 10$ models) spanning 1861–2005 (table S1). Each physics version of a model was considered a separate model. The analysis was limited to the common time period of overlap for all models and realizations (1861–2005). Those with a start year later than 1861 were not included in the analysis. We used a simple area-weighted average to create zonal means at a 5° interval (*27*).

CMIP5 1% CO_2 increase experiments

We used the CMIP5 1% per year CO_2 experiment multimodel simulation ensemble ($N = 35$ realizations, $M = 26$ models; table S2). Each physics version of a model was considered a separate model. The simulations are all initialized using a preindustrial control simulation and are of varying length. The analysis was limited to the maximum length (140-year) time interval common to all but one simulation in the archive. We used a simple area-weighted average to create zonal means at a 5° interval.

CMIP5 future projections (RCP 2.6 and RCP 8.5)

We used the CMIP5 RCP 8.5 ($N = 73$ realizations, $M = 39$ models; table S3) multimodel simulations for the analyses in the main article. Each physics version of a model was considered a separate model. The analysis was limited to the common time period of overlap for all models and realizations (2006–2099). We used a simple area-weighted average to create zonal means at a 5° interval. We did separate analyses using only the subset of (AIE) simulations that include both first and second indirect effects ($N = 28$ realizations, $M = 15$ models). We did additional analyses (see the Supplementary Materials) using the CMIP5 RCP 2.6 simulations ($N = 58$ realizations, $M = 29$ models; table S4) and the subset of AIE simulations ($N = 25$ realizations, $M = 11$ models).

Observational surface temperatures

We analyzed zonal mean boreal summer (JJA) average temperatures (surface air temperature over land and sea surface temperature over oceans) using each of three alternative datasets: GISTEMP (*35*) (1880–2015), HadCRUT4 (*36*) (1894–2015), and Cowtan and Way (*37*) (1894–2015). These three different datasets make alternative assumptions about how to account for historical data gaps, which is particularly important in the Arctic region that is key to this study, due to the large spatial gaps in this region coupled with the amplified high-latitude warming in the Northern Hemisphere in recent decades. The time period of analysis was constrained by continuous data availability for each latitude band. For example, the HadCRUT4 and Cowtan and Way datasets contain at least one grid cell temperature value in each latitude band across the range of interest (25°N to 75°N) from 1894 to the present. Accordingly, the grid cell coverage is relatively sparse in the early segments of the records and increases toward the present day. As with the model output, we used a simple area-weighted average to create zonal means at a 5° interval (*27*).

Thermal wind calculation

The change in zonal wind in the upper troposphere from a temperature gradient anomaly can be approximated (*38*) as

$$\Delta u = -\frac{R_{\text{air}}}{f}\ln\left(\frac{p_0}{p_{300}}\right)\frac{dT}{dy}$$

With the Coriolis frequency at the midlatitudes $f = 10^{-4}\ \text{s}^{-1}$, the specific gas constant for air $R_{\text{air}} = 287\ \text{m}^2\ \text{s}^{-2}\ \text{K}^{-1}$, a surface pressure of $p_0 = 1000$ mbar, an upper tropospheric pressure of $p_{300} = 300$ mbar, and a meridional temperature gradient anomaly of $\frac{dT}{dy} = \frac{0.5}{10}K^{\circ}(\text{lat}) = 4.5 \times 10^{-7}\ \text{K/m}$ (as observed over latitudes 55°N to 66°N in the T fingerprint; Fig. 1A), this would result in an approximate change in zonal winds of

$$\Delta u = -1.6\ \text{ms}^{-1}$$

SUPPLEMENTARY MATERIALS

Supplementary material for this article is available at http://advances.sciencemag.org/cgi/content/full/4/10/eaat3272/DC1

Fig. S1. Latitudinal profiles at 5° resolution.
Fig. S2. As Fig. 3 but for RCP 2.6 CMIP5 simulations.
Fig. S3. As Fig. 5 but for RCP 2.6 CMIP5 simulations.
Fig. S4. QRA fingerprint based on first half (1979–1997) and second half (1998–2015) of ERA reanalysis period compared with full period (1979–2015).
Table S1. CMIP5 historical climate model simulations.
Table S2. CMIP5 1%/year CO_2 simulations.
Table S3. CMIP5 RCP 8.5 future projection simulations.
Table S4. CMIP5 RCP 2.6 future projection simulations.

REFERENCES AND NOTES

1. C. Schär, P. Luigi Vidale, D. Lüthi, C. Frei, C. Häberli, M. A. Liniger, C. Appenzeller, The role of increasing temperature variability in European summer heatwaves. *Nature* **427**, 332–336 (2004).
2. G. A. Meehl, C. Tebaldi, More intense, more frequent, and longer lasting heat waves in the 21st century. *Science* **305**, 994–997 (2004).
3. J. O. Sewall, L. C. Sloan, Disappearing Arctic sea ice reduces available water in the American west. *Geophys. Res. Lett.* **31**, L06209 (2004).
4. E. M. Fischer, S. I. Seneviratne, P. L. Vidale, D. Lüthi, C. Schär, Soil moisture–atmosphere interactions during the 2003 European summer heat wave. *J. Clim.* **20**, 5081–5099 (2007).
5. S. Rahmstorf, D. Coumou, Increase of extreme events in a warming world. *Proc. Natl. Acad. Sci. U.S.A.* **108**, 17905–17909 (2011).
6. Intergovernmental Panel on Climate Change (IPPC), Managing the risks of extreme events and disasters to advance climate change adaptation, in *A Special Report of Working Groups I and II of the Intergovernmental Panel on Climate Change*, C. B. Field,

V. Barros, T. F. Stocker, D. Qin, D. J. Dokken, K. L. Ebi, M. D. Mastrandrea, K. J. Mach, G.-K. Platter, S. K. Allen, M. Tignor, P. M. Midgley, Eds. (Cambridge Univ. Press, 2012), 582 pp.
7. K. E. Trenberth, J. T. Fasullo, Climate extremes and climate change: The Russian heat wave and other climate extremes of 2010. *J. Geophys. Res.* **117**, D17103 (2012).
8. J. A. Francis, S. J. Vavrus, Evidence linking Arctic amplification to extreme weather in mid-latitudes. *Geophys. Res. Lett.* **39**, L06801 (2012).
9. D. Coumou, S. Rahmstorf, A decade of weather extremes. *Nat. Clim. Change* **2**, 491–496 (2012).
10. S. Westra, L. V. Alexander, F. W. Zwiers, Global increasing trends in annual maximum daily precipitation. *J. Clim.* **26**, 3904–3918 (2013).
11. V. Petoukhov, S. Rahmstorf, S. Petri, H. J. Schellnhuber, Quasiresonant amplification of planetary waves and recent Northern Hemisphere weather extremes. *Proc. Natl. Acad. Sci. U.S.A.* **110**, 5336–5341 (2013).
12. D. Coumou, A. Robinson, S. Rahmstorf, Global increase in record-breaking monthly-mean temperatures. *Clim. Change* **118**, 771–782 (2013).
13. N. Christidis, G. S. Jones, P. A. Stott, Dramatically increasing chance of extremely hot summers since the 2003 European heatwave. *Nat. Clim. Change* **5**, 46–50 (2015).
14. D. Coumou, V. Petoukhov, S. Rahmstorf, S. Petri, H. Joachim Schellnhuber, Quasi-resonant circulation regimes and hemispheric synchronization of extreme weather in boreal summer. *Proc. Natl. Acad. Sci. U.S.A.* **111**, 12331–12336 (2014).
15. J. Lehmann, D. Coumou, K. Frieler, A. V. Eliseev, A. Levermann, Future changes in extratropical storm tracks and baroclinicity under climate change. *Environ. Res. Lett.* **9**, 084002 (2014).
16. K. E. Trenberth, J. T. Fasullo, T. G. Shepherd, Attribution of climate extreme events. *Nat. Clim. Change* **5**, 725–730 (2015).
17. J. Lehmann, D. Coumou, K. Frieler, Increased record-breaking precipitation events under global warming. *Clim. Change* **132**, 501–515 (2015).
18. D. Coumou, J. Lehmann, J. Beckmann, The weakening summer circulation in the Northern Hemisphere mid-latitudes. *Science* **348**, 324–327 (2015).
19. N. S. Diffenbaugh, D. L. Swain, D. Touma, Anthropogenic warming has increased drought risk in California. *Proc. Natl. Acad. Sci. U.S.A.* **112**, 3931–3936 (2015).
20. R. E. Petrie, L. C. Shaffrey, R. T. Sutton, Atmospheric response in summer linked to recent Arctic sea ice loss. *Q. J. R. Meteorol. Soc.* **141**, 2070–2076 (2015).
21. M. P. Hoerling, M. P. Hoerling, J. P. Kossin, T. C. Peterson, P. A. Stott, Explaining extreme events of 2014 from a climate perspective. *Bull Am. Meteorol. Soc.* **96**, S1–S172 (2015).
22. V. Petoukhov, S. Petri, S. Rahmstorf, D. Coumou, K. Kornhuber, H. J. Schellnhuber, Role of quasiresonant planetary wave dynamics in recent boreal spring-to-autumn extreme events. *Proc. Natl. Acad. Sci. U.S.A.* **113**, 6862–6867 (2016).
23. E. K. M. Chang, C.-G. Ma, C. Zheng, A. M. W. Yau, Observed and projected decrease in Northern Hemisphere extratropical cyclone activity in summer and its impacts on maximum temperature. *Geophys. Res. Lett.* **43**, 2200–2208 (2016).
24. F. E. L. Otto, G. J. van Oldenborgh, J. Eden, P. A. Stott, D. J. Karoly, M. R. Allen, The attribution question. *Nat. Clim. Change* **6**, 813–816 (2016).
25. R. M. Horton, J. S. Mankin, C. Lesk, E. Coffel, C. Raymond, A review of recent advances in research on extreme heat events. *Curr. Clim. Change Rep.* **2**, 242–259 (2016).
26. K. Kornhuber, V. Petoukhov, S. Petri, S. Rahmstorf, D. Coumou, Evidence for wave resonance as a key mechanism for generating high-amplitude quasi-stationary waves in boreal summer. *Clim. Dyn.* **49**, 1961–1979 (2016).
27. M. E. Mann, S. Rahmstorf, K. Kornhuber, B. A. Steinman, S. K. Miller, D. Coumou, Influence of anthropogenic climate change on planetary wave resonance and extreme weather events. *Sci. Rep.* **7**, 45242 (2017).
28. K. Kornhuber, V. Petoukhov, D. Karoly, S. Petri, S. Rahmstorf, D. Coumou, Summertime planetary wave resonance in the Northern and Southern Hemispheres. *J. Clim.* **30**, 6133–6150 (2017).
29. J. G. Charney, J. De Vore, Multiple flow equilibria in the atmosphere and blocking. *J. Atmos. Sci.* **36**, 1205–1216 (1979).
30. B. J. Hoskins, D. J. Karoly, The steady linear response of a spherical atmosphere to thermal and orographic forcing. *J. Atmos. Sci.* **38**, 1179–1196 (1981).
31. B. J. Hoskins, T. Ambrizzi, Rossby wave propagation on a realistic longitudinally varying flow. *J. Atmos. Sci.* **50**, 1661–1671 (1993).
32. V. Petoukhov, S. Rahmstorf, S. Petri, H. J. Schellnhuber, Reply to Screen and Simmonds: From means to mechanisms. *Proc. Natl. Acad. Sci. U.S.A.* **110**, E2328 (2013).
33. I. Manola, F. Selten, H. de Vries, W. Hazeleger, "Waveguidability" of idealized jets. *J. Geophys. Res.* **118**, 10432–10440 (2013).
34. IPPC, Summary for Policymakers, in *Climate Change 2013: The Physical Science Basis. Contribution of Working Group I to the Fifth Assessment Report of the Intergovernmental Panel on Climate Change*, T. F. Stocker, D. Qin, G. K. Plattner, M. Tignor, S. K. Allen, J. Boschung, A. Nauels, Y. Xia, V. Bex, P. M. Midgley, Eds. (Cambridge Univ. Press, 2013), 27 pp.
35. J. Hansen, R. Ruedy, M. Sato, K. Lo, Global surface temperature change. *Rev. Geophys.* **48**, RG4004 (2010).
36. C. P. Morice, J. J. Kennedy, N. A. Rayner, P. D. Jones, Quantifying uncertainties in global and regional temperature change using an ensemble of observational estimates: The HadCRUT4 data set. *J. Geophys. Res.* **117**, 1–22 (2012).
37. K. Cowtan, R. G. Way, Coverage bias in the HadCRUT4 temperature series and its impact on recent temperature trends. *Q. J. R. Meteorol. Soc.* **140**, 1935–1944 (2014).
38. J. R. Holton, in *Introduction to Dynamic Meteorology* (Academic Press Inc., ed. 4, 2004), p. 545.

Acknowledgments: We acknowledge the World Climate Research Programme's Working Group on Coupled Modelling, which is responsible for CMIP, and we thank the climate modeling groups for producing and making available their model output. **Funding:** D.C. and K.K. were supported by the BMBF. **Author contributions:** M.E.M. conceived, designed, and performed the research and wrote the paper. K.K., B.A.S., and S.K.M. performed some aspects of the research and cowrote the paper. S.P. contributed Fig. 1B. D.C. and S.R. helped in the design of the research and cowrote the paper. **Competing interests:** The authors declare that they have no competing interests. **Data and materials availability:** All data needed to evaluate the conclusions in the paper are present in the paper and/or the Supplementary Materials. Additional data related to this paper may be requested from the authors. All raw data, MATLAB code, and results from our analysis are available at the supplementary website (www.meteo.psu.edu/holocene/public_html/supplements/SciAdvances2018/).

Submitted 14 February 2018
Accepted 17 September 2018
Published 31 October 2018
10.1126/sciadv.aat3272

Citation: M. E. Mann, S. Rahmstorf, K. Kornhuber, B. A. Steinman, S. K. Miller, S. Petri, D. Coumou, Projected changes in persistent extreme summer weather events: The role of quasi-resonant amplification. *Sci. Adv.* **4**, eaat3272 (2018).

ScienceAdvances

Projected changes in persistent extreme summer weather events: The role of quasi-resonant amplification

Michael E. Mann, Stefan Rahmstorf, Kai Kornhuber, Byron A. Steinman, Sonya K. Miller, Stefan Petri and Dim Coumou

Sci Adv **4** (10), eaat3272.
DOI: 10.1126/sciadv.aat3272